Published in final edited form as:
J Biol Inorg Chem. 2014 February ; 19(2): 191–205. doi:10.1007/s00775-013-1059-4.

Comparison of Divalent Transition Metal Ion ParaCEST MRI Contrast Agents

Sarina J. Dorazio, **Abiola O. Olatunde**, **Pavel B. Tsitovich**, and **Janet R. Morrow**
Department of Chemistry, University at Buffalo, Amherst, New York, 14260 USA

Janet R. Morrow: jmorrow@buffalo.edu

Abstract

Transition metal ion-based paraCEST agents (TM-CEST) are a promising new class of compounds for MRI contrast. Members in this class of compounds include paramagnetic complexes of Fe^{II}, Co^{II} and Ni^{II}. The development of the coordination chemistry for these paraCEST agents is presented with an emphasis on the choice of azamacrocycle backbone and pendent groups with the goals of controlling oxidation state, spin state and stability of the complexes. CEST spectra and images are compared for different macrocyclic complexes containing amide or heterocyclic pendent groups. The potential of paraCEST agents that function as pH and redox-activated MRI probes is discussed.

Keywords

Contrast agent; MRI; ParaCEST; Transition metal

Introduction

Magnetic resonance imaging (MRI) is used in the clinic for non-invasive diagnosis and prognosis of disease. Differences in proton density and relaxation between pathological and healthy tissues allow anatomical features to be resolved.[1] Standard MRI techniques map water proton nuclear spins through pulse sequences that distinguish protons according to differences in T_1, or longitudinal relaxation time constants, or T_2, or transverse relaxation time constants [2, 3]. The primary advantages of MRI in comparison to other imaging modalities are the excellent depth penetration and spatial resolution (up to 1 mm) of soft tissues while using non-ionizing radiation [3, 4]. One disadvantage of the MRI technique is its inherent insensitivity. For this reason, MRI typically involves monitoring the nuclear ^1H spin of the abundant water signal rather than biomolecules that are present at much lower concentrations in the body.

One method to further differentiate tissue in an MR image is to introduce a contrast agent (CA) which alters the water signal through relaxation or chemical exchange processes. Clinically approved CAs shorten the longitudinal (T_1) or transverse (T_2) relaxation times of water protons and once administered, are always “on.” The first T_1 CA, $[Gd(DTPA)(H_2O)]^{2-}$, was approved in 1988, followed by other paramagnetic polyamino carboxylate complexes [5]. Pre- and post-injection scans are currently used with clinically approved CAs, a practice which is both time-consuming and costly. Utilizing the more recent chemical exchange saturation transfer (CEST) mechanism produces CAs which rely on a selective radio frequency (RF) pulse to turn contrast “on,” while RF applied at non-resonant

Correspondence to: Janet R. Morrow, jmorrow@buffalo.edu.

frequencies results in no contrast [6]. The potential of CEST CAs is promising as shown by recent efforts to develop these agents for clinical applications. Glucose and iopamidol have been studied as CEST CAs, in part because these compounds are already certified as safe for human use [7–9]. Clinical applications for these compounds as CEST agents are being pursued.

Exogenous CEST CAs fall within the following categories which include: diamagnetic (diaCEST), paramagnetic (paraCEST), liposomal (lipoCEST), and hyperpolarized gas (hyperCEST).[10–12] Our focus in this minireview is on paramagnetic metal ion complexes that are used as paraCEST MRI contrast agents. These paraCEST agents shift the exchangeable proton and the corresponding CEST signal away from the interfering signal from magnetization transfer background produced in tissue. Until recently, trivalent lanthanides (Ln^{III}) were the only paramagnetic metal ions used as paraCEST agents. However, it is well-known that many transition metal ions have magnetic properties that enable induction of large proton shifts, with limited broadening of proton resonances [13, 14], properties which are suitable for paraCEST agents. The development of new types of paraCEST agents is motivated in part by their unique features such as their responsiveness to pH and temperature [6], metabolites [15–17], enzymes [18], redox environment [19], or oxygen [20, 21].

This minireview will focus on the development of divalent transition metal ion complexes as azamacrocycle-based paraCEST contrast agents (TM-CEST), specifically those of Fe^{II} (ferroCEST) [22–24], Ni^{II} (NiCEST) [25], and Co^{II} (CoCEST)[21, 26] (Scheme 1). The rich coordination chemistry of these first row transition metal ions along with numerous opportunities to synthesize new types of ligands makes this a fertile area for research. Notably, the coordination chemistry of these transition metal ions is quite different from that of the Ln^{III} ions. This leads to new challenges in the design of the contrast agents, but also provides opportunities for applications that are well-suited to the properties of transition metal ions.

Choice of Macrocycle Framework for paraCEST Agents

Azamacrocycles including 1,4,7-triazacyclononane (TACN); 1,4,7,10-tetraazacyclododecane (CYCLEN); 1,4,8,11-tetraazacyclotetradecane (CYCLAM); or 1,4,10-trioxa-7,13-diazacyclopentadecane appended with additional donor groups coordinate to metal ions and form highly thermodynamically stable complexes in aqueous solution [27]. These encapsulated metal ion complexes are also frequently kinetically inert to metal ion release, even in the presence of other ligands or competing metal ions, providing a blueprint for the design of exogenous MRI contrast agents[28, 29]. TACN derivatives may be appended with groups to yield six donors for hexadentate coordination to create octahedral or pseudo-octahedral complexes with many divalent transition metal ions [30]. In contrast, Ln^{III} typically have coordination numbers of nine or ten, in which the CYCLEN macrocycle with four pendent groups provides eight coordination sites, with additional sites for coordination of innersphere water molecules [28, 31, 32]. CYCLAM derivatives preferentially bind smaller metal ions due to the 6-membered rings formed between the metal ion and coordination to nitrogens [33]. This is important because metal ions prefer different chelate ring sizes, depending on their effective ionic radius [27]. The formation of a five-membered ring versus a six-membered ring between the metal ion and coordinating donor atoms, as exemplified in CYCLEN and CYCLAM complexes, influences stability of the resulting complex.

Metal ions prefer certain macrocycle cavities above others, expressed in the thermodynamic stability of a complex as a formation constant (log K values) [27]. For example, TACN

derivatives and modified CYCLAM ligands do not optimally bind Ln^{III} due to size considerations (Ln^{III} ~ 1.1 Å), but bind strongly to various divalent first-row transition metal ions (0.6–0.9 Å) [27, 34, 35]. On the other hand, CYCLEN is a more versatile framework for binding both transition metal ions and Ln^{III} upon variation of pendent groups [23, 33, 36, 37]. CYCLEN-based complexes discussed here are useful for the comparison of transition metal with Ln^{III} paraCEST agents.

Amide-appended paraCEST agents: structures and hyperfine shifts

The 1,4,7,10-(carbamoylmethyl)-1,4,7,10-tetraazacyclododecane (TCMC) ligand and metal ion complexes (Scheme 1) have been well established in the literature [36–39]. Ln^{III} complexes of TCMC and derivatives comprise a majority of the paraCEST CAs under development [6]. A crystal structure of the nine-coordinate $[Yb(TCMC)(H_2O)]^{3+}$ is shown in Figure 1 alongside the eight-coordinate $[Mn(TCMC)]^{2+}$ complex. No crystal structures are available of Fe^{II} or Co^{II} analogs, but similarity of the effective ionic radii of Fe^{II} and Co^{II} (r = 0.92 and 0.90 Å, respectively) with Mn^{II} (r = 0.96 Å) [35] suggests that these complexes may also have coordination numbers greater than six. In support of this, the proton NMR spectrum of the Fe^{II} derivative shows six distinct macrocyclic CH proton resonances of similar intensity, consistent with apparent C4 symmetry through coordination of all pendent groups (Figure 2) [23]. The Co^{II} complex of TCMC has a proton NMR spectrum in D_2O which has highly broadened macrocyclic proton resonances due to a dynamic process, making it difficult to study pendent group coordination[26]. The Ni^{II} complex of TCMC is expected to be similar to Zn^{II} [36] which contains only two bound pendent groups, based on its smaller ionic radius (0.69 and 0.74 Å, respectively) [35].

Hyperfine proton shifts arise from anisotropic arrangement of unpaired electrons on the metal ion which influence nuclear spins *via* contact (through-bond) and pseudocontact (through-space) interactions [41, 42]. Ln^{III} *4f* electrons are effectively shielded by the outer *5s* and *5p* orbitals, resulting in bonding interactions that are largely electrostatic and shifts which are predominantly pseudocontact [43]. Transition metal ion complexes typically have more covalency in their bonds than do Ln^{III} complexes, and consequently may exhibit large contact shift contributions for nuclei that are be separated by several bonds [13, 14]. These differences are evident in the hyperfine shifts of the amide protons in Ln^{III} versus transition metal ion complexes. For instance, in the presence of Yb^{III}, the amide groups on the ligand TCMC give ^1H NMR peaks at −15 and −18 ppm in aqueous solution, just 3 ppm apart [37]. The same ligand coordinated to paramagnetic Fe^{II} yields peaks at 57 and 3 ppm in CD_3CN [23], 54 ppm apart for inequivalent amide protons (Figure 2). A similar trend has been observed with other amide containing complexes of Fe^{II} [44]. These different values arise from a combination of contact and pseudocontact contributions that make prediction of hyperfine shifts more challenging for Fe^{II} than for Ln^{III}. In addition to TCMC, other amide-appended macrocyclic complexes with Fe^{II}, Ni^{II}, and Co^{II} will be discussed (Scheme 1).

TCMT complexes of Fe^{II}, Ni^{II}, and Co^{II} have been fairly well characterized [45]. While only the crystal structure of $[Ni(TCMT)]^{2+}$ is published, all three complexes are likely to be 6-coordinate with pseudo-octahedral geometry (Figure 3). IR stretching frequencies are consistent with coordination to the carbonyl oxygens of the amide pendent groups [45]. In contrast to complexes of TACN-based macrocycles, first row transition metal ions typically lie in the plane of tetrasubstituted CYCLAM ligands. Divalent transition metal ions coordinated to tetrasubstituted CYCLAM derivatives may further coordinate through two pendent groups. The two coordinating pendent groups may be either 1,4 or 1,8-amino substitutents. Conformations include ones that have two pendent groups coordinated on the same side of the ring (*cis*-conformation) or opposite (*trans*-conformation) [33, 46]. In the case of $[Ni(CCRM)]^{2+}$, spectral data is consistent with two bound pendents, as observed for

the tetracarboxylate analog $[Ni(TETA)]^{2+}$ [47]. Spectral data for $[Co(CCRM)]^{2+}$ is also consistent with coordination of two pendent groups[26].

Diaza crown ethers bind transition metal ions of varying sizes [48–51]. Addition of pendent groups to the secondary amines gives 7-coordinate pentagonal bipyramidal Ni^{II} or Co^{II} complexes, as indicated by crystal structures of benzimidazole [51] or aniline-appended derivatives [50]. Co^{II} and Ni^{II} complexes of NOPE exhibit fourteen narrow ^1H resonances. The simplicity of the NMR spectra of these complexes is consistent with C_2 symmetry in a complex of pentagonal bipyramidal geometry (Figure 4B) [25].

A complicating feature of TM-CEST agents is that the peak widths of the ^1H NMR resonances may change with coordination geometry [13]. This is especially true for Ni^{II} complexes. Broadening of proton resonances is directly influenced by electronic relaxation time (T_{1e}), field strength, and T_2 relaxivity. Octahedral Ni^{II} complexes have characteristically longer T_{1e} (~10^{-10} s) compared to other geometries, which may contribute to the broad peaks that are observed for $[Ni(CCRM)]^{2+}$ and $[Ni(TCMT)]^{2+}$ [25]. Dynamic processes on the NMR time scale also may contribute to the broad proton resonances observed for these metal ion complexes. The 7-coordinate $[Ni(NOPE)]^{2+}$ complex, by contrast, produces narrow proton resonances (full-width half-maximum (FWHM) of 150–400 Hz) [25]. This is attributed to a low T_{1e}, and to the formation of a relatively rigid complex. T_{1e} remains more consistent (~10^{-12}–10^{-11} s) for Fe^{II} and Co^{II} complexes with different geometries [13].

ParaCEST agents with appended heterocycles: structures and hyperfine shifts

Macrocycles containing heterocyclic amine donor groups are a class of ligands which are uniquely suited for transition metal ion based paraCEST agents. We discuss three different types of heterocyclic pendent groups including pyridine, benzimidazole and pyrazole. Our primary focus in this review is on TACN-based macrocyclic complexes.

There is a cornucopia of different heterocyclic pendent groups that might be used to form macrocyclic ligands for transition metal complexes. The aromatic π-system of the heterocycle plays a crucial role in bonding and in the distribution of unpaired spin, which is important both for coordination chemistry and for hyperfine shift enhancement. The latter property is especially valuable for transition metal ion complexes for which contact contribution alters paramagnetic shifts significantly. The ring size and functionalization of the ring may be varied to modulate the rigidity of the macrocyclic complex and to increase kinetic inertness [24, 40]. Finally, the presence of additional ionizable groups other than the donor atoms may provide pH responsive agents as well as modulating the overall charge and solubility of the complex [21, 24].

Pyridine derivatives are one class of heterocyclic pendent group that have been employed for TM-CEST agents [22, 24]. Pyridines are relatively soft ligands that have both sigma donor and pi acceptor properties (pK_a of 5.2 for unsubstituted pyridine) suitable for stabilizing transition metal ions in +2 oxidation states. For example, early work showed that a TACN-based ligand containing three 2-picolyl pendants (PT in Scheme 2) stabilizes low spin Fe^{II} [52]. Crystallographic studies show that $[Fe(PT)]^{2+}$ has a pseudo-octahedral coordination sphere. The complex cation has local C_3 symmetry with the pyridine nitrogens and the TACN nitrogens each forming a plane perpendicular to the axis of symmetry. The twist angle of the planes is 48.9º, closer to the 60º twist that would be observed for an octahedral complex. The methyl group of MPT and AMPT (Schemes 1 and 2) serves to produce high spin Fe^{II} by increasing the iron-nitrogen bond lengths as observed for

analogous complexes [53]. The proton resonances of $[Fe(AMPT)]^{2+}$ span the range of −20 to 190 ppm and are much sharper than any of the TACN-based amide complexes (Figure 4A). The nine sharp (FWHM = 70–350 Hz) proton resonances indicate a C_3 symmetry and a single conformer. $[Fe(MPT)]^{2+}$ also has dispersed and sharp proton resonances [40].

A second type of pendent heterocycle contains the benzimidazole group. Benzimidazoles with 2-substitutents are good donor groups with a pK_a of 6.2 for the coordinating nitrogen in 2-methyl-benzimidazole [54]. TACN derivatives with three benzimidazole pendents bind divalent transition metal ions through six nitrogen donor groups, with three heterocyclic amine protons for the production of a CEST effect. The sole reported crystal structure, that of $[Ni(BZT)]^{2+}$, has a distorted octahedral geometry (Figure 5A) with the benzimidazole pendents splayed outwards like propeller blades [55]. This suggests that steric interactions of the pendent groups may be an important feature in the relative rigidity of the complex, as shown by ^{1}H NMR studies of $[Fe(BZT)]^{2+}$ [24].

The TPT ligand contains three pyrazole donor groups and complexes with several transition metal ions [56, 57]. The crystal structure of $[Fe(TPT)]^{2+}$ shows a C_3 axis of symmetry with all six nitrogen donor atoms bound in a nearly trigonal prismatic geometry (Figure 5B). A comparison of Fe^{II}, Ni^{II} and Zn^{II} TPT structures shows that the twist angle between the planes formed by the TACN nitrogens and the pyrazole nitrogens increases as the size of the metal ion decreases, giving a geometry close to trigonal prismatic for the Fe^{II} complex and antiprismatic for the Zn^{II} complex (Figure 5C). This shows that, even within this series of closely sized metal ions, there are differences in geometry that will affect both the hyperfine shifts of the protons and the CEST properties of the complexes.

Aqueous chemistry, spin state and oxidation state of TM-CEST agents

Ligand field strength is an important factor when considering the design of divalent transition metal ion complexes for paraCEST. Low spin (LS) or high spin (HS) states in d^4–d^7 octahedral or pseudo-octahedral compounds are produced based on the ligand environment or field strength. In some cases, such as in Co^{III} or Fe^{II} (d^6), the HS species are paramagnetic, while the LS species are diamagnetic. Amide appended macrocycles produce a relatively weak-field, generally promoting the HS state of the metal ion. This makes amide pendents well-suited for transition metal-based paraCEST agents. In contrast, heterocyclic pendent groups may produce stronger field ligands to give a LS complex, as observed for $[Fe(PT)]^{2+}$. TACN derivatives with five membered heterocyclic rings including benzimidazole[24] and pyrazole[56] and with six-membered heterocycles containing methyl-pyridine pendents[22, 40] form HS Fe^{II} complexes.

An additional consideration regarding transition metal ions is the accessibility of their different oxidation states. In the case of air-sensitive Fe^{II} aqua complex (E^o = 770 mV vs NHE) and hexaamminated Co^{II} (E^o = 100 mV vs NHE) in acidic aqueous solution, oxidation to +3 can be readily achieved [58]. Alternatively, aquated Co^{II} (E^o = 1940 mV vs. NHE) and Ni^{II} (E^o = 2290 mV vs. NHE) are much more difficult to oxidize [58, 59]. Variation of the ligand can alter these values dramatically. For instance, in the case of Fe^{II}, the tricarboxylate-appended TACN ligand, 1,4,7-triazacyclononane-1,4,7-triacetate (NOTA), destabilizes the +2 state (E^o = 195 mV vs. NHE) [60] in comparison to TCMT, TCMC, STHP and PT which stabilize divalent iron (E^o = 860, 800, 1085, 970 mV vs. NHE, respectively) [23, 40]. Co^{II} complexes of macrocycles with amide donor groups (TCMC, TCMT, NOPE, CCRM) are stable in the presence of oxygen, suggestive of a large positive reduction potential [26]. In comparison to anionic carboxylate groups, neutral amide groups favor the divalent oxidation state of iron and cobalt [60]. The heterocyclic pyrazole donor

stabilizes the trivalent state as pendent groups on TACN to give $[Co(TPT)]^{3+}$ as the stable complex in aerated aqueous solution [21].

In addition to ^1H NMR analysis, assigning a value for effective magnetic moment (μ_{eff}) of transition metal-based paraCEST agents is essential for verifying oxidation and spin state of the metal ion. Solution magnetic susceptibility is measured by the Evan's method and converted to μ_{eff}. Values for FerroCEST agents, CoCEST agents and NiCEST agents are consistent with HS complexes [22, 23, 25, 26, 40].

Complex stability, dissociation and anion interactions

The stability of the TM-CEST agents is an important consideration for future *in vivo* applications. A few of the ferroCEST agents have been characterized for thermodynamic stability. These include $[Fe(TCMT)]^{2+}$ (log K = 13.5), $[Fe(TCMC)]^{2+}$ (log K = 7.5), $[Fe(STHP)]^{2+}$ (log K = 9.3) and $[Fe(PT)]^{2+}$ (log K = 19.2) where K is the formation constant of the neutral macrocycle and Fe^{II} [22, 23, 40]. The kinetic inertness of the complexes toward dissociation is another important consideration. Complexes that are kinetically slow to dissociate need not have extremely large formation constants in order for them to remain intact under physiologically relevant conditions. All of the paraCEST agents shown in Scheme 1 are inert towards dissociation at neutral pH, at 37 ºC, in the presence of carbonate and phosphate for several hours up to several days [21, 23, 25, 26, 40]. Some of the complexes dissociate more rapidly upon incubation under acidic conditions or in the presence of large excesses of competing transition metal ions such as Cu^{II} or Zn^{II}. However certain complexes, including $[Fe(TCMC)]^{2+}$, $[Co(TCMT)]^{2+}$, $[Co(TPT)]^{2+}$, $[Ni(TCMT)]^{2+}$ and $[Fe(MPT)]^{2+}$ show little to no dissociation even under these stringent conditions [21–23, 25, 26, 40].

All of the complexes in Scheme 1 are cationic and might be expected to interact with anions with a resulting change in the hyperfine-shifted proton resonances. However, the majority of the complexes shown in Scheme 1, with the exception of $[Ni(NOPE)]^{2+}$ and $[Fe(STHP)]^{2+}$, do not show changes in ^1H NMR spectra in the presence of carbonate or phosphate [22, 23, 25, 26, 40]. Studies were also conducted to monitor the effect of oxygen and reactive oxygen species on paraCEST agents that contain Fe^{II} and Co^{II}. None of the Fe^{II} complexes monitored produced substantial amounts of reactive oxygen species in the presence of peroxide and ascorbate as studied by several assays including hydroxylation of benzoate, consumption of ascorbate and plasmid DNA cleavage [40]. The lack of reactivity of these complexes towards oxygen and peroxide is consistent with both the large positive reduction potential that shows stabilization of the divalent state, and the encapsulation of the metal ion by these macrocycles.

These initial studies are promising, but much research remains to be done for the study of TM-CEST agents under more biologically relevant conditions and ultimately *in vivo*. At this juncture, it is reasonable to predict that these transition metal complexes will have suitable properties for applications as *in vivo* CAs upon optimization of coordination chemistry. A notable recent example is the $[Co(TPT)]^{2+}$ complex which produces a strong CEST signal in serum even upon incubation at 37 ºC over a 48 hour period [21].

Features of CEST

For CEST contrast, the CA must contain exchangeable protons such as NH, OH, or metal-bound H_2O. The chemical shift difference between bulk water and the exchangeable proton resonance ($\Delta\omega$, in Hz) (Figure 6) must be larger than the exchange rate constant (k_{ex}, s^{-1}) [6]. When $\Delta\omega \geq k_{ex}$, distinct signals are observed in the NMR spectrum in which the slow-to-intermediate exchange regime on the NMR timescale is maintained. In addition to these

parameters, experimental conditions such as the concentration of the CA (typically mM) and power of the presaturation pulse (B_1) generally yield greater CEST effects as they increase, but for *in vivo* studies, both of these parameters should remain low for safety reasons[10, 20]. Recent strategies to increase the CEST effect by lowering concentration of CA while increasing the number of exchangeable protons include incorporation into dendrimers [62, 63], nanoparticles [64], and liposomes [65, 66]. In addition, adding a paramagnetic metal ion with properties which promote large proton hyperfine shifts (large $\Delta\omega$) is one strategy toward creating CEST CAs with improved contrast-to-noise *in vivo*. A large $\Delta\omega$ value reduces interference from MT between endogenous macromolecules and water. MT is most intense near the bulk water signal, so that paraCEST agents with large $\Delta\omega$ compete less with background signal. When $\Delta\omega$ is small, close proximity of the water and labile proton resonances can result in "spillover" between the signals, usually observed as a broad shoulder of the water peak in a CEST spectrum. A large $\Delta\omega$ is also beneficial to allow for the greater proton exchange rate constants that modulate CEST peak intensity.

Chemical exchange of labile protons of a CEST CA with bulk water can be encoded through application of RF irradiation at the resonant frequency of the exchangeable proton. Indirect detection of the CA is achieved through monitoring the water signal intensity (M_z/M_o %) as a function of frequency offset (ppm). Chemical exchange of saturated labile CA protons is also observed in the NMR CEST spectrum. Upon direct saturation of water, minimum intensity is observed for a CEST signal, and this point is referenced as 0 ppm (Figure 6). M_z represents z-magnetization of water at a specific frequency offset when a presaturation pulse is applied, while M_o is the magnetization in which no saturation occurs (maximum water signal intensity).

ParaCEST agents: Ln^{III} complexes

A few milestones in the development of Ln^{III} paraCEST agents will be summarized here for comparison with TM-CEST agents. The first reported example in 2001 showed that a water ligand bound to $[Eu(DOTAM\text{-}glyOEt)]^{3+}$ produced a CEST peak at close to 50 ppm (Scheme 3) [67]. One of the surprizing features of this complex at the time was the relatively slow rate constant for exchange of the water ligand [68]. Slow exchange on the NMR time scale facilitated the application of this complex as a paraCEST agent. This Eu^{III} complex and similar derivatives of the TCMC (or DOTAM) ligand have been the focus of many studies that are geared towards the development of paraCEST agents as summarized in a recent review [6]. Of particular interest is the modification of pendent groups to modulate the exchange rate constant of the water ligand [69–71]. Modification of pendent groups may change the residence time of the water by several orders of magnitude. This type of paraCEST agent has also been of fundamental importance to the development of responsive agents for biological environment [72]. Eu^{III} paraCEST agents have been functionalized to enable binding to analytes such as glucose[73], lactate[16], nitric oxide[74] or metal cations such as Zn^{2+} [75]. Other responsive amide containing paraCEST agents have pendent groups that are designed for switching states as a function of pH, biological reductant or oxygen concentration[19, 20, 76–78]. A drawback to using Eu^{III} amide-appended paraCEST agents is their relatively moderate $\Delta\omega$ for the water CEST peak. To address this, analogous complexes of more highly paramagnetic Ln^{III} ions have been prepared. Examples include a Dy^{III} complex of TCMC that produced a CEST peak at −725 ppm [79]. Additional Ln^{III} ions that have large magnetic susceptibilities such as Tb^{III} also have water peaks that are shifted several hundred ppm from bulk water [80]. However, CEST peaks are quite broad. The relatively large water proton T_1 relaxivities of these Ln^{III} may decrease the magnitude of the CEST effect [77].

The amide NH protons of Ln^{III} complexes of TCMC or DOTAM derivatives give rise to CEST effects. Amide groups have the advantage that the N-alkyl substitutent can be readily varied in order to tune the exchange rate constant of the remaining NH proton [76, 81]. In addition, the Δω for amide NH protons can be changed by employing different Ln^{III} ions. Dy^{III} and Tm^{III} complexes of DOTAM-gly have CEST peaks of 77 and −51, respectively, attributed to amide NH protons[77]. A macrocyclic complex of Tm^{III} that contains bulky *t*-butyl groups on the amide pendent has a highly shifted CEST peak at −100 ppm [82]. This study shows that adding pendent groups that give a higher proportion of one diastereromeric form of the complex, the twisted square antiprismatic (TSAP) geometry, produces more highly shifted NH resonances. The large Δω allows for higher CEST contrast in the presence of the large magnetization transfer effect in tissue or in tissue-like media such as agarose.

Aside from amides, there are few other types of donor groups that have been used for Ln^{III} paraCEST agents. The only other example with four of the same donor group is found in the $[Ln(STHP)]^{3+}$ complexes that have four alcohol pendent groups (Ln^{III} = Ce^{III}, Eu^{III} and Yb^{III}) [31, 83–85]. Unfortunately, the CEST peaks of these agents are not highly shifted and the complex with the most highly shifted CEST peak, $[Yb(STHP)]^{3+}$, produces CEST only at acidic pH values. The addition of carboxylate pendents to give HPDO3A gives a Yb^{III} complex with more highly shifted CEST alcohol OH peaks at 71 ppm and 100 ppm at neutral pH [86]. Analogous complexes with three carboxylate pendents and a fourth pendent with exchangeable protons include those with amino groups in AEDO3A[87], ACDO3A [88], and APDO3A[78]. [Yb(AEDO3A)] produces CEST peaks at ca 45 and 90 ppm, while the Eu^{III} derivatives of these three macrocycles have CEST peaks that are shifted less than 40 ppm from bulk water.

There are several important lessons from the development of Ln^{III} paraCEST agents that apply to the design of TM-CEST agents. The first involves the difficulty of creating paraCEST agents that give highly shifted CEST peaks or large Δω. For Ln^{III} complexes, the exchangeable proton is shifted primarily by dipolar or through-space contributions to the hyperfine shift. Thus it is challenging to obtain large Δω without the proton resonance being unduly broadened from close proximity to the Ln^{III}. This restriction is eased partially for TM-CEST agents that have larger contact shift contributions than do Ln^{III} paraCEST agents. Second, the tunability of rate constants is desirable. Rate constants should be as large as possible while retaining slow exchange with water on the NMR time scale, but also must be optimized for pulse power [70]. In general, faster rate constants correlate to stronger CEST effects at higher radiofrequency presaturation pulse power, but there are power deposition limits that must be considered for animal studies [89]. Third, diastereomeric forms of the macrocyclic complexes can increase the number of CEST peaks as well as influence Δω. The reliance on CYCLEN based macrocycles for Ln^{III} makes it important to consider the two major diastereromeric forms that are have relatively close energies, giving a mixture of isomers for many Ln^{III} complexes [69]. For TM-CEST agents, there are many macrocyclic backbones that might be used other than CYCLEN (Scheme 1). Also, pendent groups that are inherently rigid such as 2-picolyl or benzimidazole faciliate the preparation of complexes that exist as one isomer in solution [22, 24].

Given these challenges, it is of interest to compare the CEST properties of TM-CEST agents reported to date. TM-CEST agents include complexes that have ligands used to form Ln^{III} complexes such as TCMC and STHP as well as complexes with ligands that are better suited for transition metal ions that prefer six nitrogen donor groups such as found in TPT and BZT.

TM-CEST agents

The CEST peak positions for TM-CEST agents reported to date range from 135 ppm to −19 ppm (Figures 7 & 8, Table 2). Only the most highly shifted CEST peaks are listed for the amide complexes in Table 2. As discussed above, TM-CEST agents with amide groups have multiple CEST peaks due to the inequivalence of the two amide NH protons and these protons generally have quite large chemical shift differences. Notably, $[Fe(STHP)]^{2+}$ and the amide-appended Fe^{II}, Co^{II} and Ni^{II} complexes of TCMT and NOPE and are highly symmetric. This symmetry is expected to produce two sets of three equivalent amide protons in TCMT, two sets of two equivalent amide protons in NOPE complexes and four equivalent alcohol protons in $[Fe(STHP)]^{2+}$. The single CEST peak in spectra of Fe^{II} and Co^{II} complexes of TCMC suggest that there is a single type of amide pendent group, consistent with C4 symmetry. However, as discussed above, the proton NMR of both complexes shows evidence of dynamic processes [21, 24], and in the case of $[Co(TCMC)]^{2+}$, of lower than C4 symmetry[26]. The CEST spectrum of $[Ni(CCRM)]^{2+}$ shows only two CEST peaks, consistent with two sets of two equivalent amide protons while that of $[Co(CCRM)]^{2+}$ is consistent with four distinct amide protons[26]. In contrast, TACN derivatives with heterocyclic pendents each give a single CEST peak, corresponding to their C_3 symmetry [21, 22, 24]. The CEST peak positions for the TM-CEST agents are not readily predicted without further investigation of structure combined with theoretical calculations. The exchangeable proton resonances for which we have the most information are those of the amide group. TCMT complexes of Ni^{II}, Fe^{II}, and Co^{II} give CEST peaks at 76, 69 and 32 ppm, respectively, TCMC complexes of Fe^{II} and Co^{II} are at 50 and 45 ppm, and NOPE complexes of Ni^{II} and Co^{II} are at 72 and 59 ppm, respectively. The unusual $[Co(CCRM)]^{2+}$ complex has the most highly shifted CEST peaks of the amide complexes at 112 ppm. Thus the CEST peak differences for amide groups vary by 44 ppm, 5 ppm and 13 ppm within a series of structurally similar complexes with different transition metal ions. While fewer complexes are on hand for comparison, the CEST peaks in the three distinct heterocyclic pendents in $[Fe(AMPT)]^{2+}$, $[Fe(BZT)]^{2+}$ and $[Co(TPT)]^{2+}$ are 6.5, 53 and 135 ppm, respectively (Figure 8). Clearly, the diversity of heterocyclic pendent structures will allow for large variations in CEST peak position.

The different paraCEST agents give variable CEST peak intensities (Table 2 and Figure 7). Factors that influence CEST signal intensity include the number of equivalent exchangeable protons on a paraCEST agent, the concentration of the paraCEST agent, T_1 relaxivity, and the rate constant for proton exchange, k_{ex} [90]. Another important consideration is the existence of dynamic processes on the NMR time scale, because interconversion between macrocyclic complex isomers may broaden the exchangeable proton resonances [24]. Ideally, the CEST peak should be relatively sharp to enable more complete saturation of the proton magnetization. Given these variables, the following trends are found. $[Fe(TCMC)]^{2+}$ has a slightly more intense CEST peak than does $[Fe(TCMT)]^{2+}$, consistent with the higher number of exchangeable protons in the former. However, the CEST intensity of the Co^{II} analogs are reversed, which may be attributed to the likelihood of a fewer than four coordinated pendent groups in $[Co(TCMC)]^{2+}$. Co^{II} and Ni^{II} complexes of NOPE give unexpectedly large CEST peaks for two exchangeable protons. This may be related to their rigid structure which gives rise to very sharp proton resonances and narrow CEST peaks in addition to their relatively low T_1 relaxivity. $[Co(CCRM)]^{2+}$ has relatively intense CEST peaks that most likely arise from single distinct protons, corresponding to its favorably low T_1 and rigid structure. $[Fe(STHP)]^{2+}$ gives a broad, shallow CEST peak, resulting from a relatively large rate constant that leads to exchange broadening. $[Co(TPT)]^{2+}$ has three exchangeable protons that exchange rapidly (9,200 s^{-1}). This large rate constant is accommodated by the large $\Delta\omega$ of 135 ppm for this complex. Finally, the six equivalent

protons of $[Fe(AMPT)]^{2+}$ give rise to a substantial CEST peak even at the low presaturation power that was necessary to obtain the CEST spectrum.

A topic of particular interest is the design of paraCEST agents that are responsive to biological environment, including agents for probing changes in temperature, pH and redox status. It is especially straightforward to prepare paraCEST agents that produce pH dependent CEST effects given that rate constants for proton exchange are generally pH dependent.[23, 76, 78] Amide NH and pyrazole NH exchange rate constants increase over the pH range of 6.5 to 7.5, consistent with base-catalyzed proton exchange [21, 23, 25]. Increasing rate constants lead to an increase in the CEST peak intensity, so long as the CEST peak does not undergo exchange broadening. Importantly for paraCEST agents, it is relatively straightforward to incorporate multiple types of exchangeable protons that give rise to distinct CEST peaks. The different pH dependence of each distinct CEST peak can be used in a ratiometric fashion to register pH. For example, the CEST peak intensity of the alcohol OH protons of $[Fe(STHP)]^{2+}$ have a different pH dependence than do the amide protons of $[Fe(TCMC)]^{2+}$ [23]. A complex which combined both groups would be anticipated to have two CEST peaks that might be used for ratiometric analysis of pH. Interestingly, two of the CEST peaks attributed to distinct amide protons in the $[Co(CCRM)]^{2+}$ complex each have a different pH dependence[26]. This is one of the few examples of a paraCEST agent that has two different CEST peaks that can be used for the design of a ratiometic pH probe.

MRI agents with redox potentials close to that in tissue (−100 to −300 mV)[91] may be used as redox-activated MRI agents [92]. Both Fe^{II} and Co^{II} complexes have redox potentials that can be tuned to this range. The Co^{II}/Co^{III} couple is especially readily tuned to negative redox potentials for azamacrocycles and cages [60]. Cobalt complexes with heterocyclic pendents such as $[Co(TPT]^{2+}$ are active paraCEST contrast agents when in the divalent form and inactivated in the trivalent form, opening up opportunities for modulating MRI contrast by oxygen pressure and biological reductants [21].

Phantom images

CEST imaging studies of transition metal based paraCEST agents collected on a 4.7 Tesla MRI scanner have been reported [21, 22, 25, 26]. These studies use a pulse train comprised of five Gauss pulses at 12 μT for 1 s, interpulse delay of 200 μs at +/−135 ppm. CEST phantom images were collected by subtracting the ratio of “on” resonance, for example at (73 ppm) and “off” resonance (−73 ppm) from 100 % for $[Ni(NOPE)]^{2+}$ (Figure 9). Phantom images on the Ni^{II} complexes contained 2–8 mM complex at 37 ºC to produce contrast between 4 to 20 %. Of the Ni^{II} complexes, the most intense CEST effect was observed for $[Ni(NOPE)]^{2+}$ for both NMR spectroscopy experiments (Table 2) and MR scanning (Figure 9) [25]. The $[Co(NOPE)]^{2+}$ complex was imaged down to 250 μM by using this protocol [26]. Other imaging protocols may be used including CEST-FISP (FISP = fast imaging with steady-state free precession)[93]. CEST-FISP improves data precision by averaging multiple data points. Improvements in imaging protocol both for in vitro phantoms and for in vivo systems will surely advance the application of paraCEST contrast agents *in vivo*.

Overview and Future Considerations

Transition metal ion paraCEST agents show promise for future development. Research in this area has but scratched the surface of combinations of metal ion and ligand that may produce useful new contrast agents. Many different donor groups with exchangeable protons might be used for paraCEST. Alteration of the metal ion within each complex yields

variations in geometry, CEST effect, chemical shift, and T_1 relaxivity. Three first row transition metal ions paraCEST agents have been reported and reviewed here (Figure 10). These three were chosen because they are biologically relevant metal ions as well as have suitable paramagnetic properties. Iron, in particular, may be absorbed through pathways that humans have evolved for this abundant element. Other metal ions that may have promising paraCEST properties based on their magnetic properties as shift agents include heavier transition metal ions [14]. The extensive coordination chemistry of transition metal ion complexes will be useful for expanding the field of paraCEST MRI agents for new biomedical applications.

Acknowledgments

We gratefully acknowledge the John R. Oishei Foundation, the Bruce Holm Catalyst Fund, the NIH (CA-173309) and the NSF (CHE-1310374) for support.

Abbreviations

AMPT	1,4,7-Tris[(5-amino-6-methyl-2-pyridyl)methyl]-1,4,7-triazacyclononane
B_1	, Presaturation pulse power
BZT	1,4,7-Tris(benzimidazol-2-ylmethyl)-1,4,7-triazacyclononane
CA	Contrast agent
CCRM	1,4,8,11-(Carbamoylmethyl)-1,4,8,11-tetraazacyclododecane
CEST	Chemical exchange saturation transfer
CEST-FISP	Chemical exchange saturation transfer – fast imaging with steady-state free precession
CoCEST	Co^{II} paraCEST
CYCLAM	1,4,8,11-Tetraazacyclotetradecane
CYCLEN	1,4,7,10-Tetraazacyclododecane
Δω	Chemical shift difference
diaCEST	Diamagnetic CEST
DMSO	dimethylsulfoxide
DOTA	1,4,7,10-Tetraazacyclododecane-1,4,7,10-tetraacetic acid
DOTAM	1,4,7,10-(Carbamoylmethyl)-1,4,7,10-tetraazacyclododecane or TCMC
DTPA	Diethylenetriamine pentaacetate
ferroCEST	Fe^{II} paraCEST
FWHM	Full-width half-maximum
HS	High spin
hyperCEST	Hyperpolarized gas CEST
IR	infrared
k_{ex}	Exchange rate constant
lipoCEST	Liposomal CEST
Ln^{III}	Trivalent lanthanide ion

LS	Low spin
MPT	1,4,7-Tris[(6-methyl-2-pyridyl)methyl]-1,4,7-triazacyclononane
MRI	Magnetic resonance imaging
MT	Magnetization transfer
M_o	Magnetization of water with no saturation
M_z	Magnetization upon application of presaturation pulse
μ_{eff}	Effective magnetic moment
NHE	Normal hydrogen electrode
NiCEST	Ni^{II} paraCEST
NMR	Nuclear magnetic resonance
NOPE	7,13-Bis(carbamoylmethyl)-1,4,10-trioxa-7,13-diazacyclopentadecane
NOTA	1,4,7-Triazacyclononane-1,4,7-triacetate
paraCEST	Paramagnetic
CEST PT	1,4,7-Tris(2-pyridylmethyl)-1,4,7-triazacyclononane
RF	Radio frequency
STHP	(1S,4S,7S,10S)-1,4,7,10-tetrakis(2-hydroxypropyl)-1,4,7,10-tetraazacyclododecane
T_1	Longitudinal relaxation time
T_{1e}	Electronic relaxation time
T_2	Transverse relaxation time
TACN	1,4,7,-Triazacyclononane
TCMC	1,4,7,10-(Carbamoylmethyl)-1,4,7,10-tetraazacyclododecane or DOTAM
TCMT	1,4,7-(Carbamoylmethyl)-1,4,7-triazacyclononane
TETA	1,4,8,11-Tetraazacyclotetradecane-1,4,8,11-tetraacetic acid
TM-CEST	transition metal paraCEST
TPT	1,4,7-Tris(pyrazol-3-ylmethyl)-1,4,7-triazacyclononane

References

1. McRobbie, DW.; Moore, EA.; Graves, MJ.; Prince, MR. MRI: From Picture to Proton. Cambridge University Press; Cambridge: 2007.
2. Benveniste H, Blackband S. Prog Neurobiol. 2002; 67:393–420. [PubMed: 12234501]
3. Strijkers GJ, Mulder WJM, van Tilborg GAF, Nicolay K. Anti-Cancer Agents Med Chem. 2007; 7:291–305.
4. Massoud TF, Gambhir SS. Genes Dev. 2003; 17:545–580. [PubMed: 12629038]
5. Caravan P, Ellison JJ, McMurry TJ, Lauffer RB. Chem Rev. 1999; 99:2293–2352. [PubMed: 11749483]
6. Viswanathan S, Kovacs Z, Green KN, Ratnakar SJ, Sherry AD. Chem Rev. 2010; 110:2960–3018. [PubMed: 20397688]
7. Chan KW, McMahon MT, Kato Y, Liu G, Bulte JW, Bhujwalla ZM, Artemov D, van Zijl PC. Magn Reson Med. 2012; 68:1764–1773. [PubMed: 23074027]

8. Walker-Samuel S, Ramasawmy R, Torrealdea F, Rega M, Rajkumar V, Johnson SP, Richardson S, Goncalves M, Parkes HG, Arstad E, Thomas DL, Pedley RB, Lythgoe MF, Golay X. Nat Med. 2013; 19:1067–1072. [PubMed: 23832090]
9. Longo DL, Dastru W, Digilio G, Keupp J, Langereis S, Lanzardo S, Prestigio S, Steinbach O, Terreno E, Uggeri F, Aime S. Magn Reson Med. 2011; 65:202–211. [PubMed: 20949634]
10. van Zijl PCM, Yadav NN. Magn Reson Med. 2011; 65:927–948. [PubMed: 21337419]
11. Stevens TK, Palaniappan KK, Ramirez RM, Francis MB, Wemmer DE, Pines A. Magn Reson Med. 2013; 69:1245–1252. [PubMed: 22791581]
12. Zaiss M, Schnurr M, Bachert P. J Chem Phys. 2012; 136:144106. (142012). doi: 144110.141063/144101.3701178. [PubMed: 22502500]
13. Bertini, I.; Luchinat, C. NMR of Paramagnetic Molecules in Biological Systems. The Benjamin/Cummings Publishing Company, Inc; Menlo Park: 1986.
14. Bertini I, Luchinat C, Parigi G, Pierattelli R. Chem Bio Chem. 2005; 6:1536–1549.
15. Ren J, Trokowski R, Zhang S, Malloy CR, Sherry AD. Magn Reson Med. 2008; 60:1047–1055. [PubMed: 18958853]
16. Aime S, Delli Castelli D, Fedeli F, Terreno E. J Am Chem Soc. 2002; 124:9364–9365. [PubMed: 12167018]
17. Hammell J, Buttarazzi L, Huang C-H, Morrow JR. Inorg Chem. 2011; 50:4857–4867. [PubMed: 21548563]
18. Yoo B, Raam MS, Rosenblum RM, Pagel MD. Contrast Media Mol Imaging. 2007; 2:189–198. [PubMed: 17712869]
19. Ratnakar SJ, Viswanathan S, Kovacs Z, Jindal AK, Green KN, Sherry AD. J Am Chem Soc. 2012; 134:5798–5800. [PubMed: 22420507]
20. Song B, Wu Y, Yu M, Zhao P, Zhou C, Kiefer GE, Sherry AD. Dalton Trans. 2013; 42:8066–8069. [PubMed: 23575743]
21. Tsitovich PB, Spernyak JA, Morrow JR. Angew Chem. 2013 in press.
22. Dorazio SJ, Tsitovich PB, Siters KE, Spernyak JA, Morrow JR. J Am Chem Soc. 2011; 133:14154–14156. [PubMed: 21838276]
23. Dorazio SJ, Morrow JR. Inorg Chem. 2012; 51:7448–7450. [PubMed: 22757664]
24. Tsitovich PB, Morrow JR. Inorganica Chim Acta. 2012; 393:3–11.
25. Olatunde AO, Dorazio SJ, Spernyak JA, Morrow JR. J Am Chem Soc. 2012; 134:18503–18505. [PubMed: 23102112]
26. Dorazio SJ, Olatunde AO, Spernyak JA, Morrow JR. Chem Commun. 2013; 49:10025–10027.
27. Hancock RD, Martell AE. Chem Rev. 1989; 89:1875–1914.
28. Amin S, Voss DA Jr, Horrocks WD Jr, Lake CH, Churchill MR, Morrow JR. Inorg Chem. 1995; 34:3294–3300.
29. Pasha A, Tircso G, Benyo ET, Brucher E, Sherry AD. Eur J Inorg Chem. 2007; 2007:4340–4349. [PubMed: 19802361]
30. Wainwright KP. Coord Chem Rev. 1997; 166:35–90.
31. Huang CH, Hammell J, Ratnakar SJ, Sherry AD, Morrow JR. Inorg Chem. 2010; 49:5963–5970. [PubMed: 20509631]
32. Parker D. Chem Soc Rev. 2004; 33:156–165. [PubMed: 15026820]
33. Meyer M, Dahaoui-Gindrey V, Lecomte C, Guilard L. Coord Chem Rev. 1998; 178:1313–1405.
34. Amin S, Marks C, Toomey LM, Churchill MR, Morrow JR. Inorganica Chim Acta. 1996; 246:99–107.
35. Shannon RD. Acta Cryst. 1976; A32:751–767.
36. Maumela H, Hancock RD, Carlton L, Reibenspies JH, Wainwright KP. J Am Chem Soc. 1995; 117:6698–6707.
37. Zhang S, Michaudet L, Burgess S, Sherry AD. Angew Chem Int Ed. 2002; 41:1919–1921.
38. Wang S, Westmoreland TD. Inorg Chem. 2009; 48:719–727. [PubMed: 19072697]
39. Amin S, Morrow JR, Lake CH, Churchill MR. Angew Chem Int Ed Engl. 1994; 33:773–775.

40. Dorazio SJ, Tsitovich PB, Gardina SA, Morrow JR. J Inorg Biochem. 2012; 117:212–219. [PubMed: 22824155]
41. Pintacuda G, John M, Su X-C, Otting G. Acc Chem Res. 2007; 40:206–212. [PubMed: 17370992]
42. Peters JA, Huskens J, Raber DJ. Prog Nucl Magn Reson Spectrosc. 1996; 28:283–350.
43. Bünzli, J-CG.; Choppin, G. Lanthanide Probes in Life, Chemical, and Earth Sciences: Theory and Practice. Elsevier; Amsterdam, New York: 1989.
44. Ming L-J, Lauffer RB, Que L Jr. Inorg Chem. 1990; 29:3060–3064.
45. Weyhermuller T, Wieghardt K, Chaudhuri P. J Chem Soc, Dalton Trans. 1998:3805–3813.
46. Liang XY, Sadler PJ. Chem Soc Rev. 2004; 33:246–266. [PubMed: 15103406]
47. Studer M, Riesen A, Kaden TA. Helv Chim Acta. 1989; 72:1253–1258.
48. Vaiana L, Esteban-Gomez D, Platas-Igleslas C, Mato-Iglesias M, Avecilla F, de Blas A, Rodriguez-Blas T. Polyhedron. 2007; 26:4141–4146.
49. Regueiro-Figuero M, Esteban-Gomez D, Platas-Iglesias C, de Blas A, Rodriguez-Blas T. Eur J Inorg Chem. 2007:2198–2207.
50. Platas-Iglesias C, Vaiana L, Esteban-Gomez D, Avecilla F, Real JA, de Blas A, Rodriguez-Blas T. Inorg Chem. 2005; 44:9704–9713. [PubMed: 16363839]
51. Vaiana L, Regueiro-Figueroa M, Mato-Iglesias M, Platas-Iglesias C, Esteban-Gomez D, de Blas A, Rodriguez-Blas T. Inorg Chem. 2007; 46:8271–8282. [PubMed: 17764174]
52. Christiansen L, Hendrickson DN, Toftlund H, Wilson SR, Xie CL. Inorg Chem. 1986; 25:2813–2818.
53. Koikawa M, Jensen KB, Matsushima H, Tokii T, Toftlund H. Journal of the Chemical Society-Dalton Transactions. 1998:1085–1086.
54. Jerez G, Kaufman G, Prystai M, Schenkeveld S, Donkor KK. J Sep Sci. 2009; 32:1087–1095. [PubMed: 19306255]
55. Li Q-X, Luo Q-H, Li Y-Z, Tu Q-Y. Inorg Chim Acta. 2005; 358:504–512.
56. Di Vaira M, Mani F, Stoppioni P. J Chem Soc Dalton Trans. 1997:1375–1379.
57. Di Vaira M, Mani F, Stoppioni P. J Chem Soc Dalton Trans. 1994:3739–3743.
58. Crabb, E.; Moore, E.; Smart, L. Concepts in transition metal chemistry. Royal Society of Chemistry Open University; Cambridge, United Kingdom: 2010.
59. Sigel, A.; Sigel, H.; Sigel, RKO., editors. Nickel and Its Surprising Impact in Nature: Metal Ions in Life Sciences. Wiley; 2007.
60. Bernhardt PV, Chen K-I, Sharpe PC. J Biol Inorg Chem. 2006; 11:930–936.10.1007/s00775-006-0148-z [PubMed: 16868742]
61. Dorazio SJ, Morrow JR. Eur J Inorg Chem. 2012:2006–2014.
62. Snoussi K, Bulte JWM, Gueron M, van Zijl PCM. Magn Reson Med. 2003; 49:998–1005. [PubMed: 12768576]
63. Pikkemaat JA, Wegh RT, Lamerichs R, van de Molengraaf RA, Langereis S, Burdinski D, Raymond AYF, Janssen HM, de Waal BFM, Willard NP, Meijer EW, Grüll H. Contrast Media Mol Imaging. 2007; 2:229–239. [PubMed: 17937448]
64. Cai K, Kiefer GE, Caruthers SD, Wickline SA, Lanza GM, Winter PM. NMR Biomed. 2012; 25:279–285. [PubMed: 21751273]
65. Opina ACL, Ghaghada KB, Zhao P, Kiefer G, Annapragada A, Sherry AD. PLoS One. 2011; 6:e27370. doi:27310.21371/journal.pone.0027370. [PubMed: 22140438]
66. Aime S, Delli Castelli D, Crich SG, Gianolio E, Terreno E. Acc Chem Res. 2009; 42:822–831. [PubMed: 19534516]
67. Zhang S, Winter P, Wu K, Sherry AD. J Am Chem Soc. 2001; 123:1517–1518. [PubMed: 11456734]
68. Zhang S, Wu K, Biewer MC, Sherry AD. Inorg Chem. 2001; 40:4284–4290. [PubMed: 11487334]
69. Woods M, Pasha A, Zhao P, Tircso G, Chowdhury S, Kiefer G, Woessner DE, Sherry AD. Dalton Trans. 2011; 40:6759–6764. [PubMed: 21625687]
70. Sherry AD, Wu Y. Curr Opin Chem Biol. 2013; 17:167–174. [PubMed: 23333571]

71. Mani T, Tircso G, Togao O, Zhao P, Soesbe TC, Takahashi M, Sherry AD. Contrast Media Mol Imaging. 2009; 4:183–191. [PubMed: 19672854]
72. De Leon-Rodriguez LM, Lubag AJ, Malloy CR, Martinez GV, Gillies RJ, Sherry AD. Acc Chem Res. 2009; 42:948–957. [PubMed: 19265438]
73. Zhang S, Trokowski R, Sherry AD. J Am Chem Soc. 2003; 125:15288–15289. [PubMed: 14664562]
74. Liu G, Li Y, Pagel MD. Magn Reson Med. 2007; 58:1249–1256. [PubMed: 18046705]
75. De Leon-Rodriguez LM, Lubag AJ, Lopez JA, Andreu-de-Riquer G, Alvarado-Monzon JC, Sherry AD. Medchemcomm. 2012; 3:480–483. [PubMed: 24013159]
76. Opina AC, Wu Y, Zhao P, Kiefer G, Sherry AD. Contrast Media Mol Imaging. 2011; 6:459–464. [PubMed: 22144023]
77. Aime S, Barge A, Delli Castelli D, Fedeli F, Mortillaro A, Nielsen FU, Terreno E. Magn Reson Med. 2002; 47:639–648. [PubMed: 11948724]
78. Sheth VR, Liu G, Li Y, Pagel MD. Contrast Media Mol Imaging. 2012; 7:26–34. [PubMed: 22344877]
79. Woods M, Woessner DE, Sherry AD. Chem Soc Rev. 2006; 35:500–511. [PubMed: 16729144]
80. Aime S, Carrera C, Delli Castelli D, Geninatti Crich S, Terreno E. Angew Chem Int Ed Engl. 2005; 44:1813–1815. [PubMed: 15723362]
81. Mani T, Opina AC, Zhao P, Evbuomwan OM, Milburn N, Tircso G, Kumas C, Sherry AD. J Biol Inorg Chem. 2013
82. Stevens TK, Milne M, Elmehriki AA, Suchy M, Bartha R, Hudson RH. Contrast Media Mol Imaging. 2013; 8:289–292. [PubMed: 23606433]
83. Hammell J, Buttarazzi L, Huang CH, Morrow JR. Inorg Chem. 2011; 50:4857–4867. [PubMed: 21548563]
84. Huang CH, Morrow JR. J Am Chem Soc. 2009; 131:4206–4207. [PubMed: 19317496]
85. Huang CH, Morrow JR. Inorg Chem. 2009; 48:7237–7243. [PubMed: 19722692]
86. Ferrauto G, Delli Castelli D, Terreno E, Aime S. Magn Reson Med. 2013; 69:1703–1711. [PubMed: 22837028]
87. Krchova T, Kotek J, Jirak D, Havlickova J, Cisarova I, Hermann P. Dalton Trans. 2013
88. Chauvin T, Durand P, Bernier M, Meudal H, Doan BT, Noury F, Badet B, Beloeil JC, Toth E. Angew Chem Int Ed Engl. 2008; 47:4370–4372. [PubMed: 18454438]
89. Woessner DE, Zhang S, Merritt ME, Sherry AD. Magn Reson Med. 2005; 53:790–799. [PubMed: 15799055]
90. Zhang S, Merritt M, Woessner DE, Lenkinski RE, Sherry AD. Acc Chem Res. 2003; 36:783–790. [PubMed: 14567712]
91. Banerjee R. J Biol Chem. 2012; 287:4397–4402. [PubMed: 22147695]
92. Loving GS, Mukherjee S, Caravan P. J Am Chem Soc. 2013; 135:4620–4623. [PubMed: 23510406]
93. Shah T, Lu L, Dell KM, Pagel MD, Griswold MA, Flask CA. Magn Reson Med. 2011; 65:432–437. [PubMed: 20939092]

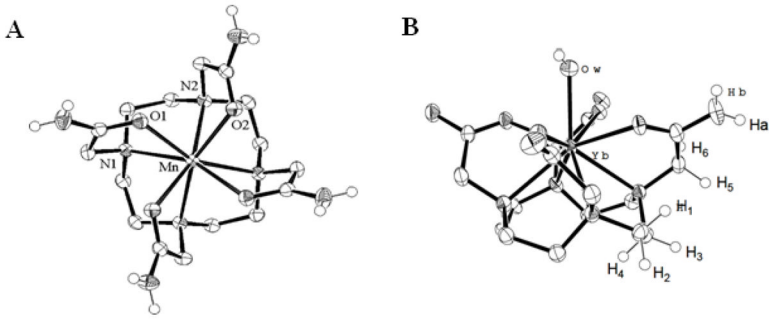

Figure 1.
Crystal structures of A) $[Mn(TCMC)]^{2+}$and B) $[Yb(TCMC)(H_2O)]^{3+}$. Reprinted with permission from references [38] and [37], respectively.

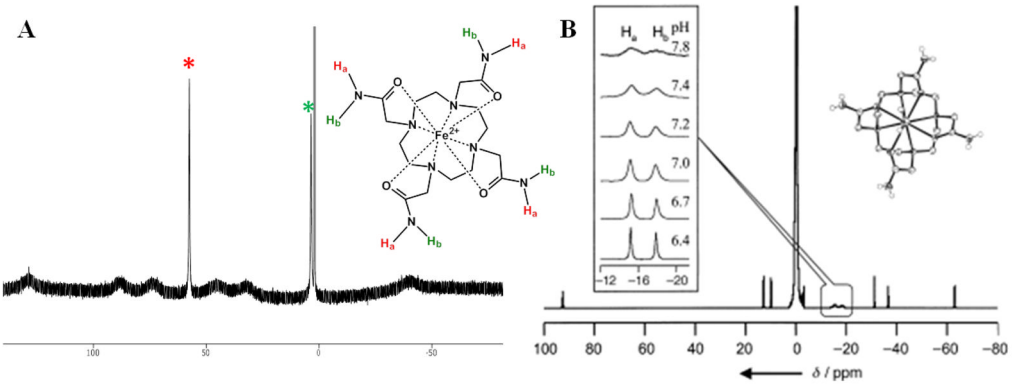

Figure 2.

A) ^{1}H NMR spectra for $[Fe(TCMC)]^{2+}$ in CD_3CN and B) $[Yb(TCMC)(H_2O)]^{3+}$ in H_2O. The * indicates the location of amide NH protons. The broad proton resonances are assigned as macrocycle CH protons. Adapted with permission from references [40] and [37].

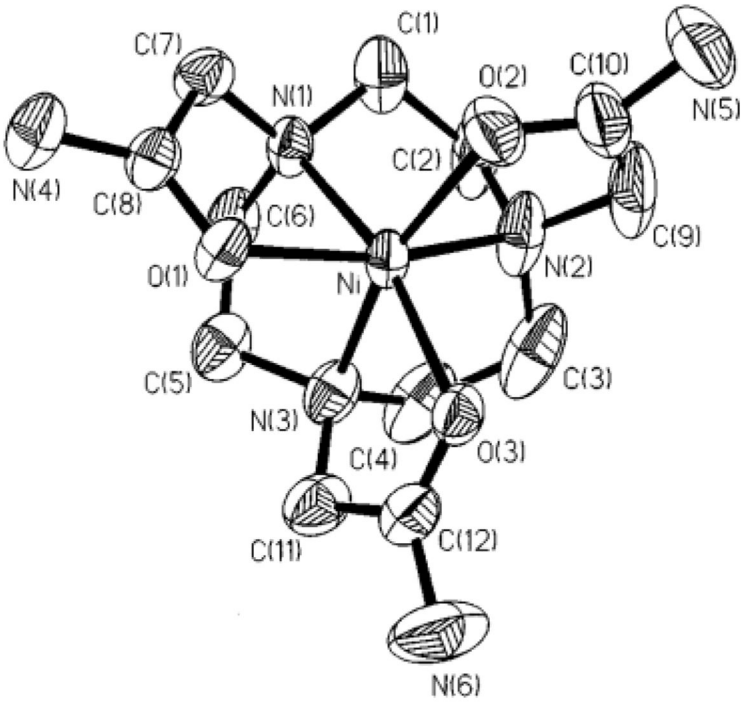

Figure 3.
Crystal structure of $[Ni(TCMT)]^{2+}$. Reprinted with permission from reference [45].

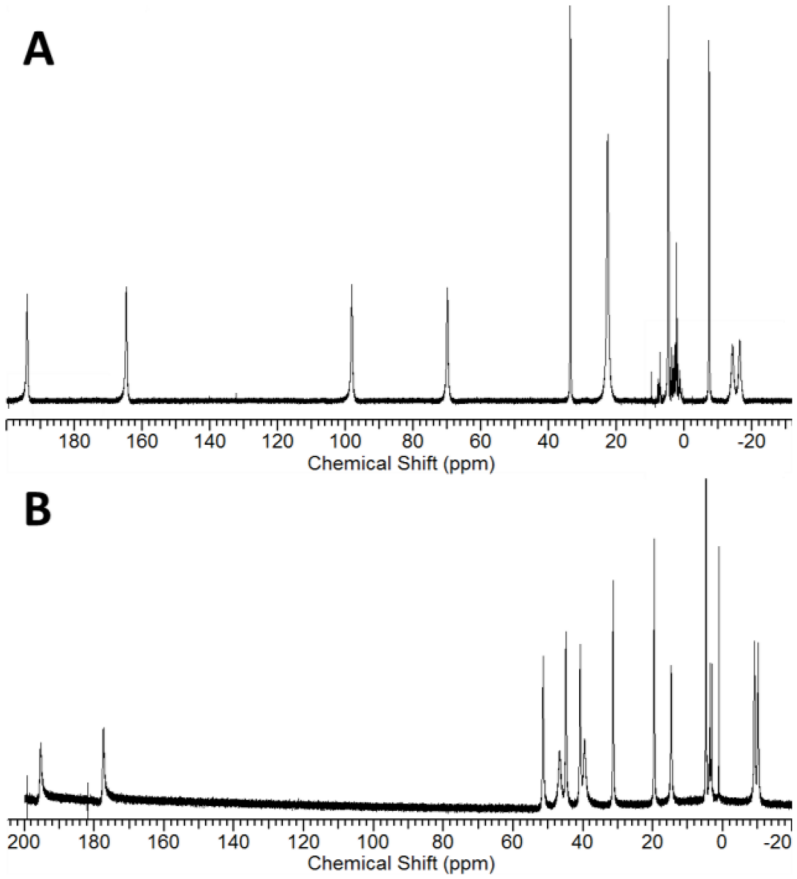

Figure 4.
A) ^{1}H NMR spectra of $[Fe(AMPT)]^{2+}$ in D_2O, pD 7.0, (B) $[Ni(NOPE)]^{2+}$ in D_2O. Adapted with permission from references [22, 25].

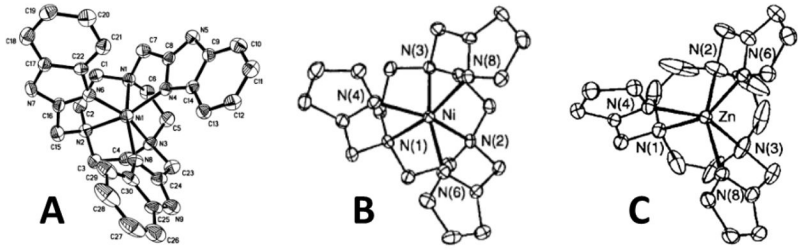

Figure 5.
Crystal structures of A) deprotonated [Ni(H$_{-2}$BZT)], (B) $[Ni(TPT)]^{2+}$ (C) $[Zn(TPT)]^{2+}$ showing complex cation geometry. Adapted with permission from references [55–57].

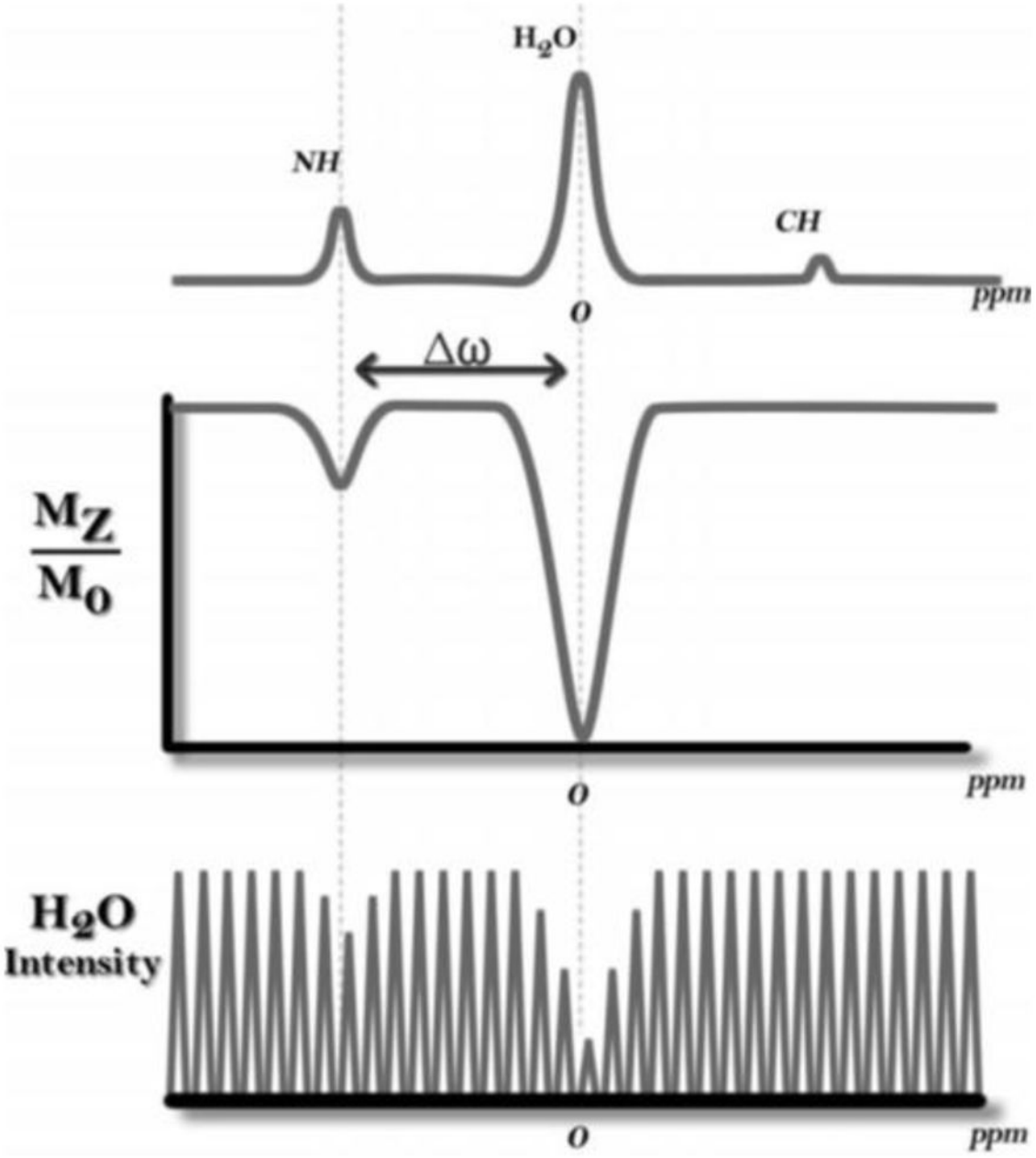

Figure 6.
Illustration of a ^{1}H NMR spectrum of a CEST agent (top), corresponding CEST spectrum (middle), and representation of water signal intensity (bottom). Reprinted with permission from reference [61].

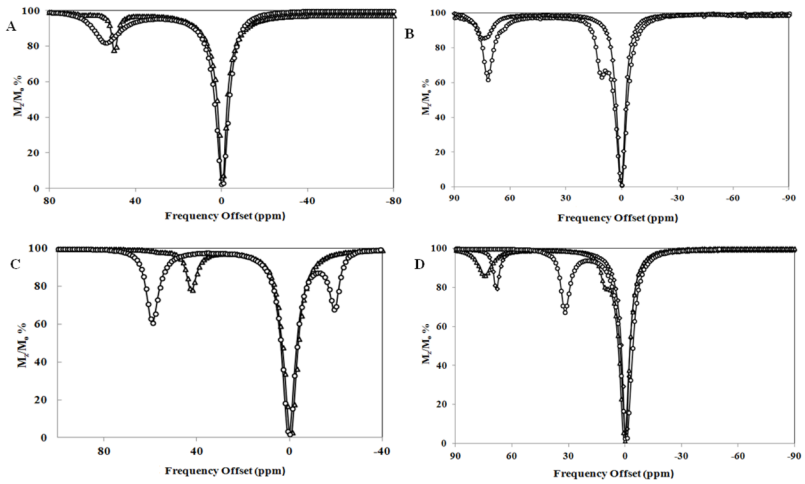

Figure 7.

CEST spectra of A) $[Fe(STHP)]^{2+}$ (○) and $[Fe(TCMC)]^{2+}$ (▲); B) $[Ni(CCRM)]^{2+}$ (◇) and $[Ni(NOPE)]^{2+}$ (○); C) $[Co(NOPE)]^{2+}$ (○) and $[Co(TCMC)]^{2+}$ (▲); D) $[Ni(TCMT)]^{2+}$ (▲), $[Fe(TCMT)]^{2+}$ (⋄), and $[Co(TCMT)]^{2+}$ (○). All samples contained 10 mM complex, 20 mM HEPES buffer pH ~7.4, and 100 mM NaCl B_1 = 24 μT (1000 Hz) presaturation for 2 s at 37 ºC,. CEST spectra modified from references [22, 23, 25, 26].

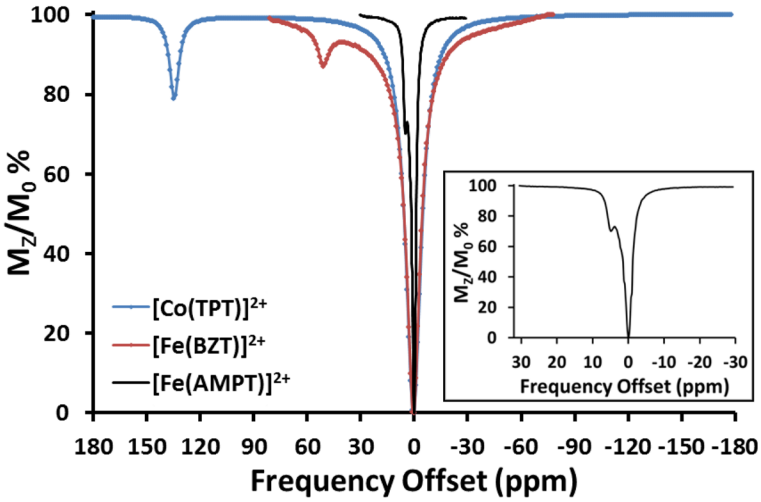

Figure 8.

CEST spectra (11.7 T NMR) of 4 mM $[Fe(AMPT)]^{2+}$ (black line), 100 mM NaCl, pH 7.0 (B_1= 11 μT, 4 s, 25 ºC); 3mM $[Fe(BZT)]^{2+}$ (red line), 100 mM NaCl, pH 6.3 (B_1= 23 μT, 3 s, 25 ºC); and 8 mM $[Co(TPT)]^{2+}$ (blue line), 100 mM NaCl, 20 mM HEPES, pH 7.0 (B_1= 24 μT, 3 s, 37 ºC). Insert shows expanded CEST spectrum of $[Fe(AMPT)]^{2+}$ [21, 22, 24].

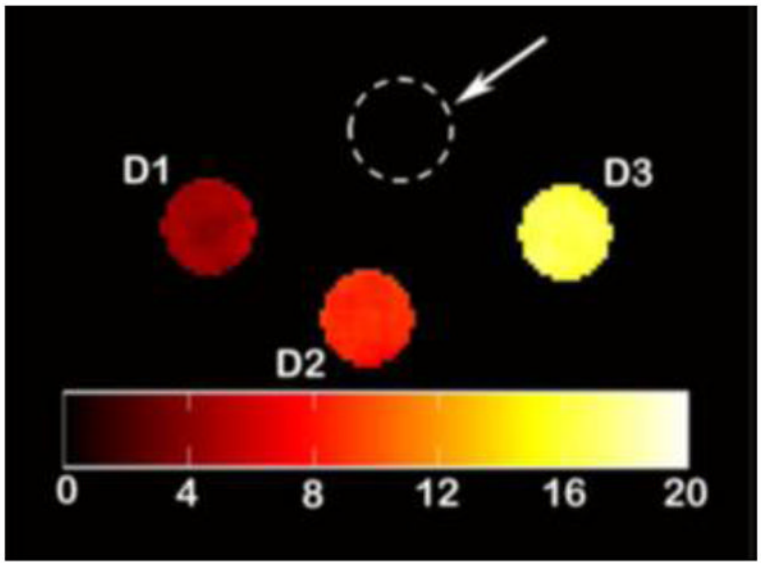

Figure 9.

Phantom images of $[Ni(NOPE)]^{2+}$ on a 4.7 T MR scanner. Center contains only 20 mM HEPES,100 mM NaCl. Concentration of $[Ni(NOPE)]^{2+}$ varies: D1 2mM, D2 4mM, and D3 8 mM with 20 mM HEPES pH~ 7.4, 100 mM NaCl at 37º C. Reprinted with permission from reference [25].

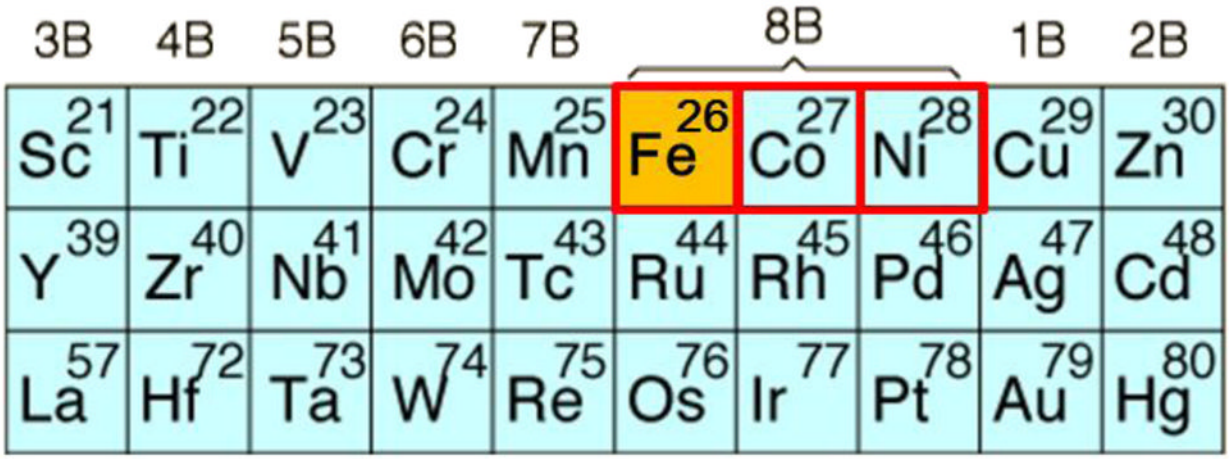

Figure 10.
Transition metal ions to date that show promise as paraCEST agents.

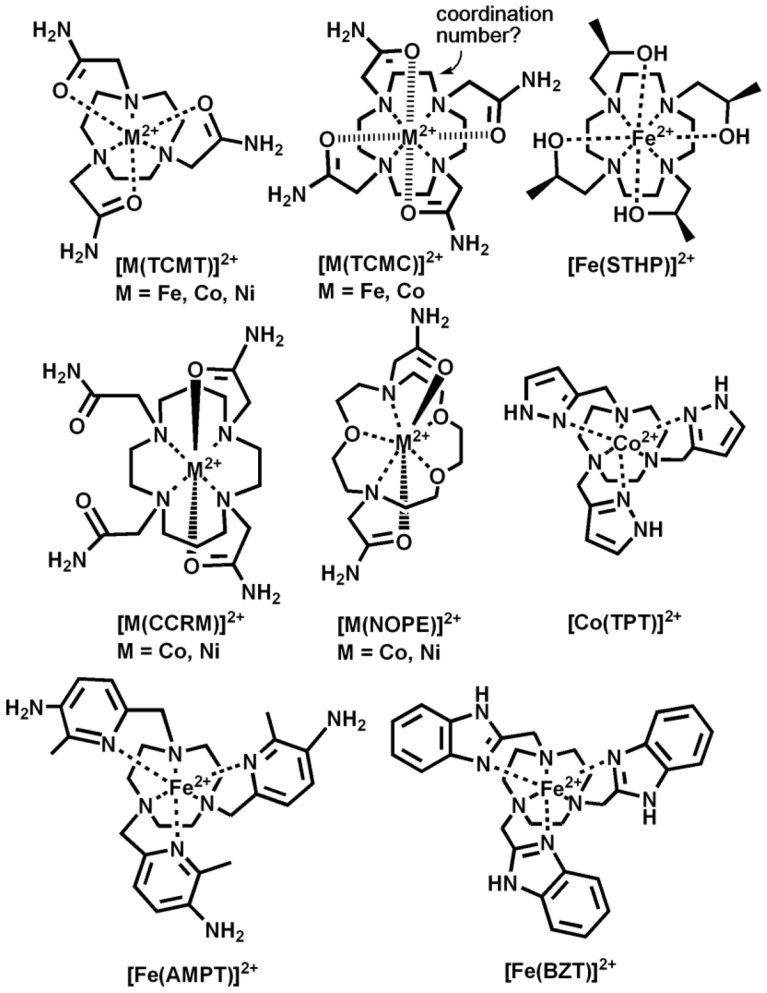

Scheme 1.
Divalent transition metal ion-based paraCEST agents.

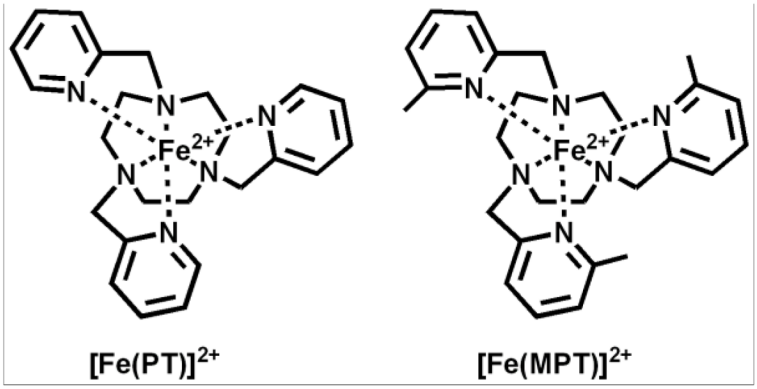

Scheme 2.
Macrocyclic complexes with pyridine pendents

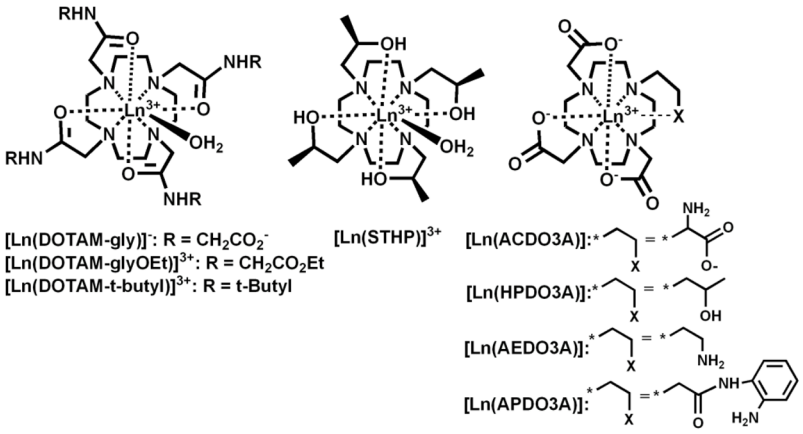

Scheme 3.
Representative Ln^{III} paraCEST agents

Table 1

Effective magnetic moment (μ_{eff}) of complexes at 25 ºC [22, 23, 25, 26, 40]

Complex	μ_{eff} (μ_B)
[Fe(TCMT)] $^{2+}$	5.1
[Fe(AMPT)]$^{2+}$	5.8
[Fe(STHP)]$^{2+}$	5.0
[Fe(TCMC)]$^{2+}$	5.3
[Ni(TCMT)]$^{2+}$	3.2
[Ni(CCRM)]$^{2+}$	3.1
[Ni(NOPE)]$^{2+}$	3.4
[Co(TCMT)]$^{2+}$	5.2
[Co(TCMC)]$^{2+}$	4.5
[Co(NOPE)]$^{2+}$	4.1
[Co(CCRM)]$^{2+}$	4.6
[Co(TPT)]$^{2+}$	5.7

Table 2

Comparison of Fe^{II}, Co^{II}, and Ni^{II} paraCEST Agents.

Complex	N[a]	m[b]	Chemical Shift (ppm)	k_{ex}[c] (s^{-1})	T_1 relaxivity[d] ($mM^{-1}\cdot s^{-1}$)	% CEST[e]
$[Fe(TCMT)]^{2+}$	6	3	69	240	0.210	19
$[Fe(AMPT)]^{2+}$	6	6	6.5	--	0.021	18
$[Fe(BZT)]^{2+}$	3	3	53	-	-	13
$[Fe(STHP)]^{2+}$	4	4	54	3000	0.232[1]	17
$[Fe(TCMC)]^{2+}$	8[f]	4[f]	50	400	0.263[1]	23
$[Ni(TCMT)]^{2+}$	6	3	76	364	0.210	13
$[Ni(CCRM)]^{2+}$	8[g]	1[g]	76	328	0.097	14
$[Ni(NOPE)]^{2+}$	4	2	72	241	0.012	39
$[Co(TCMT)]^{2+}$	6	3	32	890	0.125	33
$[Co(TCMC)]^{2+}$	8	4	45	300	0.096	21
$[Co(NOPE)]^{2+}$	4	2	59	240	0.038	38
$[Co(CCRM)]^{2+}$	8[g]	1[g]	112	510	0.008	29
$[Co(TPT)]^{2+}$	3	3	135	9200	0.093	21

[a] Total number of exchangeable protons on the paraCEST agent.

[b] Number of magnetically equivalent protons that give rise to CEST peak.

[c] Rate constant (k_{ex}) for proton exchange at 37 ºC.

[d] T_1 relaxivity on a 4.7 T MR scanner, at 37 ºC.

[e] % CEST on an 11.7 T NMR spectrometer on 10 mM complex, 20 mM HEPES pH 7.4, 100 mM NaCl, B_1=24 μT [77]presaturation 2s at 37 ºC, except for $[Fe(AMPT)]^{2+}$ (4 mM, pH 7.0, B_1 = 11 μT, 4s), $[Fe(BZT)]^{2+}$ (3 mM, pH 6.3, B_1 = 23 μT, 3s), $[Co(TPT)]^{2+}$ (8 mM, pH 7.0, B_1 = 23 μT, 3s).

[f] for coordination of all four amide pendent groups.

[g] for coordination of two pendent groups with each amide proton magnetically inequivalent.